Molecular Therapy
Nucleic Acids
Original Article

Modulation of miR-181 influences dopaminergic neuronal degeneration in a mouse model of Parkinson's disease

Colleen S. Stein,[1] Jared M. McLendon,[1] Nathan H. Witmer,[2] and Ryan L. Boudreau[1,2]

[1]Department of Internal Medicine, Iowa Neuroscience Institute, Fraternal Order of Eagles Diabetes Research Center, Abboud Cardiovascular Research Center, Carver College of Medicine, University of Iowa, Iowa City, IA, USA; [2]Program in Molecular Medicine, Carver College of Medicine, University of Iowa, Iowa City, IA, USA

Parkinson's disease (PD) is caused by the loss of dopaminergic (DA) neurons in the substantia nigra (SN). Although PD pathogenesis is not fully understood, studies implicate perturbations in gene regulation, mitochondrial function, and neuronal activity. MicroRNAs (miRs) are small gene regulatory RNAs that inhibit diverse subsets of target mRNAs, and several studies have noted miR expression alterations in PD brains. For example, miR-181a is abundant in the brain and is increased in PD patient brain samples; however, the disease relevance of this remains unclear. Here, we show that miR-181 target mRNAs are broadly downregulated in aging and PD brains. To address whether the miR-181 family plays a role in PD pathogenesis, we generated adeno-associated viruses (AAVs) to overexpress and inhibit the miR-181 isoforms. After co-injection with AAV overexpressing alpha-synuclein (aSyn) into mouse SN (PD model), we found that moderate miR-181a/b overexpression exacerbated aSyn-induced DA neuronal loss, whereas miR-181 inhibition was neuroprotective relative to controls (GFP alone and/or scrambled RNA). Also, prolonged miR-181 overexpression in SN alone elicited measurable neurotoxicity that is coincident with an increased immune response. mRNA-seq analyses revealed that miR-181a/b inhibits genes involved in synaptic transmission, neurite outgrowth, and mitochondrial respiration, along with several genes having known protective roles and genetic links in PD.

INTRODUCTION

Parkinson's disease (PD) is the second most prevalent aging-related neurodegenerative disease worldwide, affecting ~10 million individuals, the vast majority of whom are diagnosed with sporadic PD. PD patients suffer a progressive loss of dopaminergic (DA) neurons that reside in the substantia nigra (SN) and project to and release dopamine in the striatum. Disease progression coincides with the hallmark accumulation of deposited protein aggregates known as Lewy bodies. The primary component of Lewy bodies is alpha-synuclein (aSyn), a protein with poorly understood function that is often elevated in PD patient brains. The overexpression of aSyn can elicit the onset of PD and neuronal dysfunction in humans (e.g., individuals with triplication of the gene encoding aSyn,[1] *SNCA*), as well as in mice (e.g., aSyn transgenic mouse models of PD[2,3]). In addition, several groups have demonstrated that viral-mediated aSyn overexpression by the direct injection of recombinant adeno-associated virus (AAV) into rodent brains serves as a valuable model of PD that recapitulates many disease aspects (e.g., aSyn aggregation, DA neuronal degeneration, neuroinflammation, motor deficits [in some cases]).[4,5] However, the precise mechanisms of aSyn-induced neurotoxicity are not fully understood, and this has hindered the development of therapeutics for PD.

Mechanistic studies have implicated several important biological pathways/processes in PD pathogenesis, including impaired lysosomal-autophagy pathways, calcium overload, and mitochondrial dysfunction. Moreover, aberrations in transcriptional and post-transcriptional gene regulation are evident in PD mouse models and in post-mortem PD patient brains. For example, several groups have conducted small RNA profiling in PD brain samples to identify changes in microRNAs (miRs),[6,7] which serve as master regulators of the transcriptome and play critical roles in nervous system biology. The human genome encodes for ~2,000 miRs, which are non-coding RNAs that incorporate into the Argonaute (Ago)-RNA-induced silencing complex (RISC) silencing complexes to direct target mRNA silencing (e.g., transcript destabilization) typically through miR-mRNA base pairing via the seed region (positions 2–8 of the miR). These RNAs are capable of regulating a diverse set of target mRNAs to uniquely coordinate a biological response, and their potential to serve as therapeutic targets is being investigated for a broad range of diseases.[8,9]

While exploring the literature and related available datasets, we noted multiple instances in which miR-181a levels were found to be elevated in aging brain tissues,[10] as well as in PD brains and cerebrospinal fluid, with one study showing a positive correlation with Lewy body deposition.[6,7] MiR-181a is part of the miR-181a/b/c/d family, which exhibits perfect sequence conservation among most species

Received 7 January 2022; accepted 10 February 2022;
https://doi.org/10.1016/j.omtn.2022.02.007.

Correspondence: Ryan L. Boudreau, Department of Internal Medicine, University of Iowa, 4334 PBDB, Iowa City, IA 52242, USA.
E-mail: ryan-boudreau@uiowa.edu

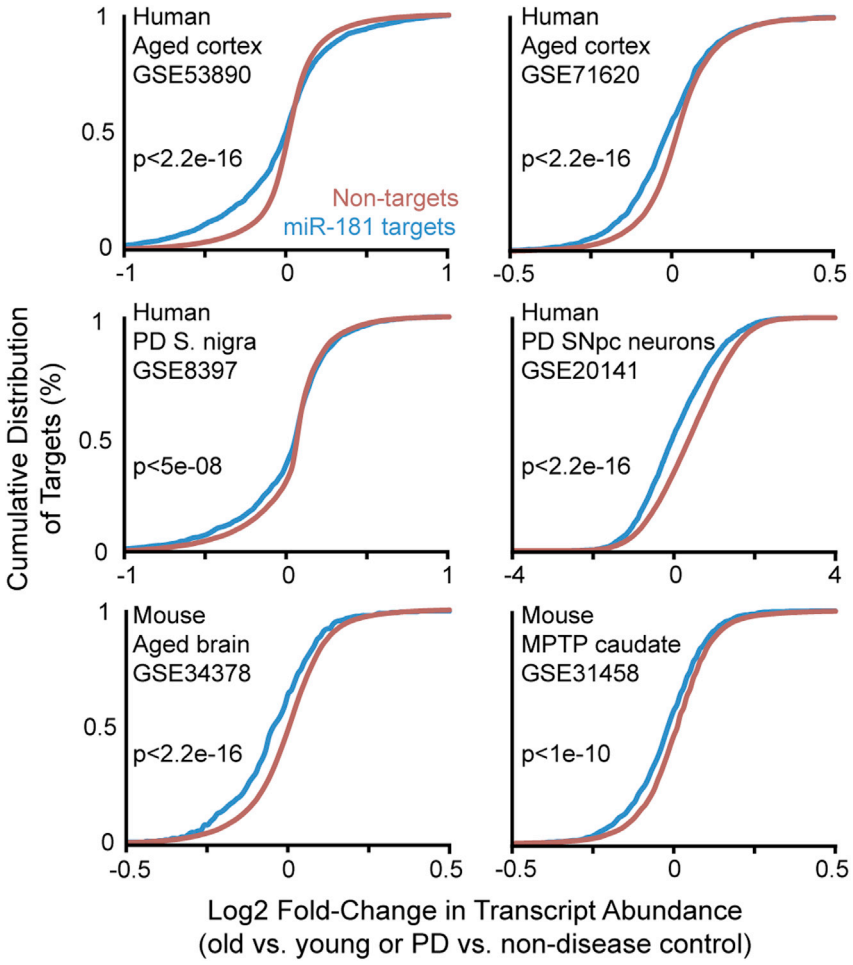

Figure 1. miR-181 target mRNAs are broadly depressed in aging and PD brains

Publicly available transcriptome-wide gene expression data from studies comparing young and old or control and PD (or PD model, 1-methyl-4-phenyl-1,2,3,6-tetrahydropyridine [MPTP]) in human and mouse brain samples were analyzed to assess mRNA levels of miR-181 targets (blue, genes having either TargetScan-predicted 3′UTR binding sites and/or empirically determined binding sites by Ago2 HITS-CLIP [crosslinking immunoprecipitation coupled with high-throughput sequencing][11,15,20]), relative to all of the other genes (red). In each of the analyzed datasets, cumulative fraction curves for miR-181 targets show leftward shifts, indicative of broad downregulation in aging brains (e.g., 18–29 versus ≥65 years old for humans and 13–26 versus 104–130 weeks old for mice), in SN and laser-captured DA neurons from the SN pars compacta (SNpc) from PD patients, relative to non-diseased controls, and in a rodent model of PD, achieved by MPTP injection. GEO accessions (GSE no.), and Kolmogorov–Smirnov (KS)-test p values are shown.

(including humans and rodents) and is predicted to engage many highly conserved target sites within shared genes across vertebrates; for example, of 1,001 miR-181/a/b/c/d target genes predicted in mice, 914 are also predicted targets in humans (per the TargetScan database[11]). The miR-181a/b/c/d family is highly enriched for expression in the nervous system, with the highest levels in post-mitotic neurons (including DA neurons), particularly for miR-181a/b;[12–14] one miR profiling study in mouse brains indicated that miR-181a is consistently expressed in the top 20 of more than 600 detected miRs across several neuronal subtypes.[14] Furthermore, we and others have shown that the miR-181 family targets several genes involved in neuronal growth and neurite extension, mitochondrial biogenesis, autophagy/mitophagy, and cell survival.[15–18] Notably, genetic and molecular inhibition of miR-181a/b is neuroprotective in fish and rodent models of genetically or chemically induced mitochondrial dysfunction, which presents with neurodegenerative phenotypes.[18] It is also neuroprotective in mice subjected to cerebral ischemia (stroke).[19] Based on these overall findings, we hypothesized that miR-181 inhibition may be neuroprotective in a PD mouse model, and we therefore tested the effects of viral-mediated gain-of-function and loss-of-function of miR-181 in a viral-based PD model of aSyn overexpression. The results of our studies support that miR-181 promotes DA neuronal degeneration and that suppressing its activity protects against aSyn-induced neurotoxicity.

RESULTS

miR-181 target mRNAs are broadly depressed in aging and PD brains

Previous reports indicate that miR-181a levels are elevated in aging and PD brain tissues;[6,7,10] however, there have been no published efforts attempting to link these changes with broad downregulation of miR-181 target genes in these settings. To address this, we analyzed publicly available data from several studies that previously evaluated transcriptomic changes in human brain samples, comparing young versus old or control versus PD tissues. Specifically, we performed cumulative fraction analyses to compare fold change distributions of miR-181 target genes against all other genes. Notably, in each dataset, we found that miR-181 mRNA targets are overall significantly shifted toward lower expression levels in aged cortex (ages 24–29 versus ≥80 years old, NCBI GEO accession: GSE53890; and, ages 18–25 versus ≥65 years old, NCBI GEO accession: GSE71620), as well as in SN tissues (NCBI GEO accession: GSE8397) and laser-microdissected DA neurons (NCBI GEO accession: GSE20141) from PD versus non-diseased control samples (Figure 1). Similar findings were also observed in aged mouse brains and (GSE34378) and mouse brains treated with a PD-related neurotoxin (GSE31458).

Generation of miR-181 overexpression and inhibition vectors

As an initial step toward testing the effects of gain-of-function and loss-of-function of miR-181 on DA neurons in the setting of PD,

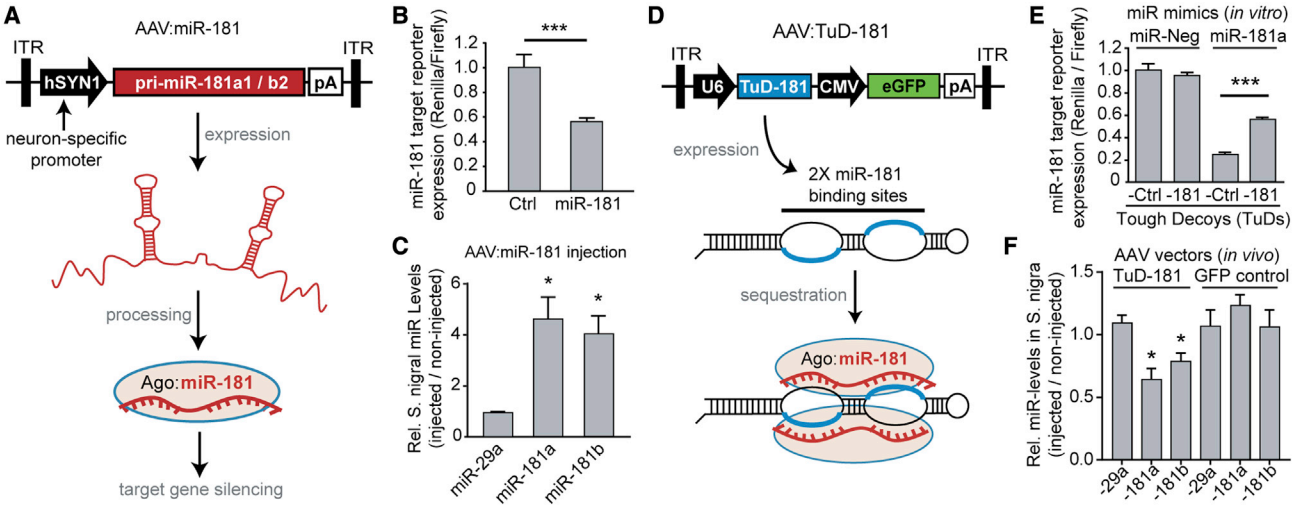

Figure 2. Overview and validation of miR-181 overexpression and inhibitor constructs

(A) Schematic of a custom AAV:miR-181 vector with a bicistronic cassette expressing primary miR stem loops for miR-181a1 and miR-181b2 under control of neuronal-specific human Synapsin-1 promoter (hSYN1). (B) *In vitro* functional validation of the miR-181a1/b2 cassette was done by co-transfecting HEK293 cells with CMVmiR-181a1b2 plasmid (miR-181) or CMV-only control (Ctrl) plasmid along with an miR-181 target reporter plasmid that co-expresses a Renilla luciferase transgene with miR-181 target sites embedded within the 3′UTR, as well as a Firefly luciferase transgene for normalization. Luciferase activities were determined at 48 h post-transfection and plotted as Renilla:Firefly ratios (n = 3–6/group). (C) *In vivo* validation was done by direct unilateral stereotaxic injection of AAV:miR-181 (1.65×10^{10} vg) into the SN of mice, and 3 weeks later, miR-181a/b and miR-29a levels were measured in RNA samples collected from SN tissues dissected from injected and contralateral non-injected control hemispheres. qPCR data were normalized to endogenous SNO135 levels and plotted as injected:non-injected ratios (n = 3/group). (D) Schematic of a custom AAV:TuD-181 vector expressing a tough decoy (TuD) miR-181 inhibitor under control of the U6 promoter and a CMV-driven GFP reporter. TuD-181 harbors 2 high-affinity miR-181 binding sites capable of sequestering miR-181 and preventing its natural function. (E) *In vitro* functional validation of the TuD-181 cassette was done by co-transfecting N2a cells, which have low endogenous miR-181, with the luciferase-based miR-181 target reporter plasmid, synthetic miRs (miR-181a or scrambled negative control, miR-Neg), and plasmids expressing either TuD-181 or a scrambled control, TuD-Ctrl. Luciferase activities were determined at 48 h post-transfection and plotted as Renilla:Firefly ratios (n = 4/group), showing that TuD-181 partially blocks the ability of synthetic miR-181a to suppress the miR-181 target reporter. (F) *In vivo* validation was done by direct unilateral stereotaxic injection of either AAV:TuD-181 or AAV:GFP control ($\sim 1.5 \times 10^{10}$ vg) into the SN of mice, and 9 weeks later, endogenous miR-181a/b levels were measured in RNA samples collected from SN tissues that were dissected from injected or contralateral non-injected control hemispheres. qPCR data were normalized to SNO135 RNA levels and plotted as injected:non-injected ratios (n = 3/group). The data in this figure are represented as the means ± SEMs. p values were obtained using either 1-way ANOVA with Tukey's multiple comparisons test (E) or 2-tailed unpaired t tests, making the indicated comparison (B) or comparing non-injected versus injected sides for each miR quantified (C and F); ***$p < 0.001$ and *$p < 0.05$.

we constructed plasmids and viral vectors to overexpress or inhibit miR-181. For overexpression, we generated a dual-hairpin miR-181a1/b2 primary miR transcript driven by either a cytomegalovirus (CMV) promoter for preliminary *in vitro* testing or a neuronal-specific human synapsin-1 gene promoter (hSYN1) for subsequent *in vivo* testing in the mouse brain (Figure 2A).[21] In cell transfection studies, the CMV-based miR-181a1/b2 plasmid increased miR-181a/b levels by >30-fold ($p < 0.001$, data not shown) and repressed the expression of a co-transfected luciferase reporter gene harboring miR-181 seed binding sites (∼50%, $p < 0.001$; Figure 2B). For *in vivo* testing, a neurotropic recombinant AAV (serotype 5) encoding the hSYN1-miR-181a1/b2 cassette was delivered unilaterally to the SN in mice via direct intraparenchymal injection. Three weeks later, this led to a >4-fold increase in miR-181a/b levels in injected SN, relative to non-injected contralateral side controls ($p = 0.001$; Figure 2C). While this experiment lacks a control AAV injection into the contralateral side, this increase is not likely the result of a general response to direct AAV injection, since miR-181a levels do not significantly increase following AAV-GFP injection (Figure 2F).

For miR-181 inhibition, we generated a U6-driven "tough decoy" (TuD) RNA that forms a highly stable stem-loop structure capable of sequestering two miR-181 molecules via high-affinity antisense binding sites (Figure 2D).[22] In cell transfection studies, the TuD-181 plasmid construct reversed the silencing of a miR-181 target luciferase reporter by ∼50% ($p < 0.0001$, relative to a scrambled control, TuD-Ctrl) in the presence of elevated miR-181 levels, which was achieved via co-transfection of synthetic miR-181 mimic oligonucleotides (Figure 2E). For *in vivo* testing, an AAV5 co-expressing U6-driven TuD-181 and a CMV-driven GFP (AAV:TuD-181) was injected unilaterally into the SN in mice. Nine weeks later, endogenous miR-181a/b levels were reduced 20%–35% in injected SN, relative to either non-injected contralateral side controls or control mice that received a unilateral injection of AAV5 expressing GFP alone (AAV:GFP; $p = 0.001$; Figure 2F), whereas the expression of another

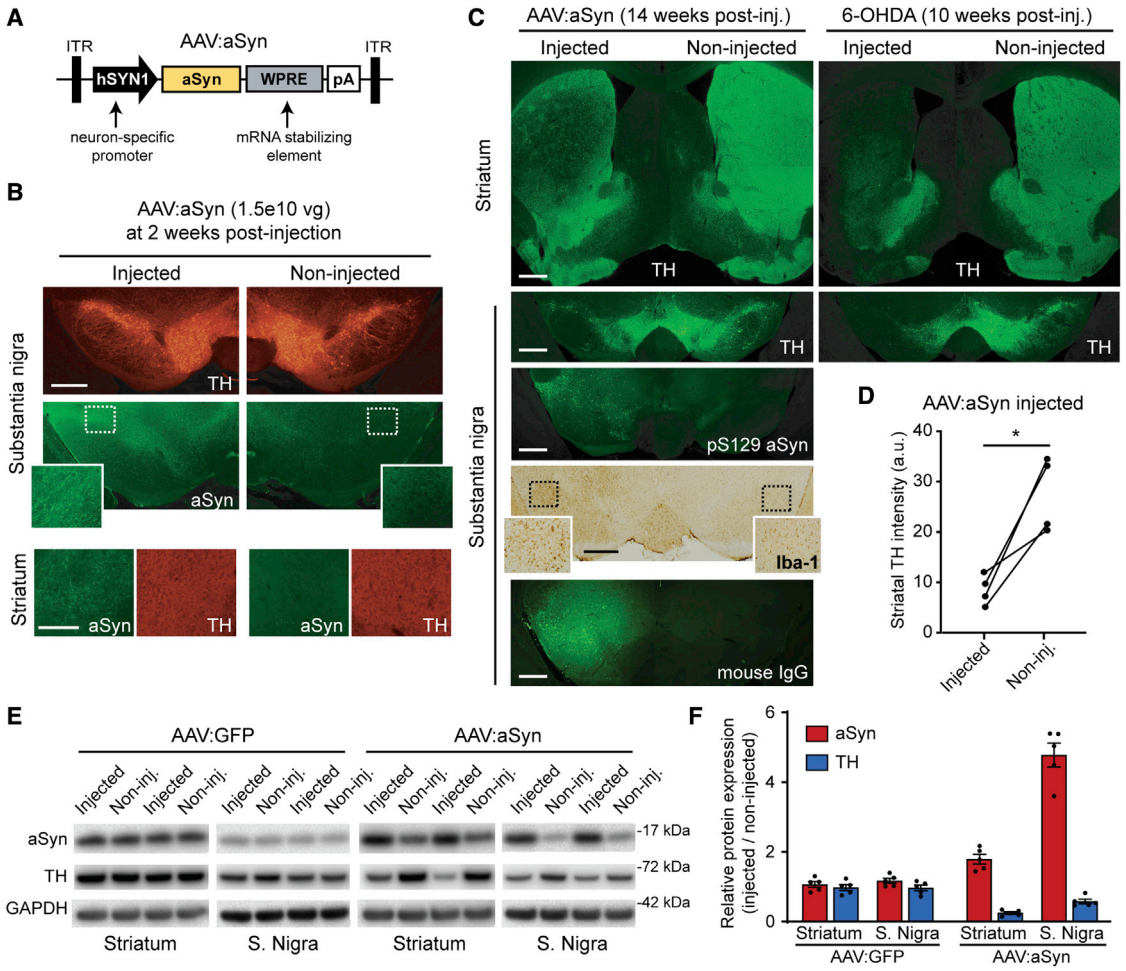

Figure 3. Characterization of an AAV-based aSyn overexpression mouse model of PD

(A) Schematic AAV:aSyn vectors expressing human aSyn under the control of the neuronal-specific human hSYN1 promoter with the WPRE mRNA stabilizing element. (B) Immunohistochemistry staining shows the expression of the human aSyn transgene and the preservation of endogenous tyrosine hydroxylase (TH) levels in mouse SN and striatum 2 weeks after the unilateral stereotaxic injection of AAV:aSyn (1.5×10^{10} vg) into the SN. (C) Immunohistochemistry staining showing reduced TH levels and elevations in phospho-S129 aSyn, activated microglia (Iba-1), and endogenous IgG in mouse brains 14 weeks after the unilateral stereotaxic injection of AAV:aSyn (1.5×10^{10} vg) into the SN. Unilateral injection with the 6-OHDA neurotoxin served as a control for the loss of DA neurons. (D) Image analysis was performed to quantify striatal TH staining intensity in AAV:aSyn-injected and contralateral non-injected control sides (n = 4 mice). The p value was obtained by a 2-tailed paired t test; *$p < 0.05$. (E and F) Elevated aSyn expression and decreased TH levels were also made evident by western blot in striatal and SN tissues harvested at 9 weeks after unilateral injection of AAV:aSyn or control AAV expressing GFP via the hSYN1 promoter (AAV:GFP; 1×10^{10} vg, n = 5/group). Representative blots are shown, and densitometry analyses were performed to quantify aSyn and TH protein levels, normalized to the GAPDH loading control. The data are represented as the means ± SEMs. All scale bars: 500 μm, except for the striatal images in (B) (scale bar: 200 μm). Related to Figure S1 and S2.

abundant brain miR, miR-29a, was not changed. These findings are noteworthy and suggest that the magnitude of miR-181 inhibition may be greater than that detected by this assay, considering that TuD RNAs act primarily through miR sequestration, as opposed to degradation.

Generation and characterization of an AAV-based aSyn overexpression mouse model of PD

To test the effects of viral-mediated gain-of-function and loss-of-function of miR-181 on PD outcomes in mice, we established an AAV-based aSyn overexpression PD model to work in our hands. For this, AAV5 encoding human aSyn driven by the neuron-specific hSYN1 promoter (AAV:aSyn) was unilaterally injected directly into the SN in mice (Figure 3A). After 2–3 weeks post-injection, aSyn expressed from the AAV5 transgene was evident in the SN by immunostaining using an antibody specific for human aSyn (Figure 3B). Western blotting SN tissue lysates for total aSyn (human transgene and endogenous mouse) showed a 4-fold increase in aSyn levels, relative to either non-injected contralateral side controls or AAV:GFP-injected mice ($p < 0.0001$, 1-way ANOVA with Tukey's

multiple comparisons test; Figure S1). At these early time points, aSyn overexpression did not adversely affect DA neurons in the SN nor their projections to the striatum, as evidenced by preserved tyrosine hydroxylase (TH) immunostaining and western blotting (Figures 3B and S1). However, at later time points (9–18 weeks), a significant loss of TH staining was found in AAV:aSyn-injected hemispheres in both the striatum (loss of DA neuronal projections) and SN (DA neuronal cell loss), and approached that obtained after unilateral injection 6-hydroxydopamine (6-OHDA, a classic nigral neurotoxin; Figures 3C and 3D). Reduced TH protein levels were substantiated by western blot, in which TH bands were overtly diminished in SN and striatal regions of AAV:aSyn mice (injected versus non-injected hemisphere) but not in AAV:GFP mice, at 9 weeks post-unilateral injection (Figures 3E and 3F). Confocal imaging revealed a coincident loss of neuronal cell bodies and TH^+ neurons in the injected SN (Figure S2A), supporting a model in which aSyn overexpression precipitates DA neuronal death. Concomitant with TH loss, striatal staining for dopamine transporter (DAT, a marker of DA neuron terminals) was reduced, while staining for DARPP-32 (a marker for medium spiny neurons) showed no difference in injected versus non-injected sides (Figure S2B). These findings are consistent with the selective loss of DA neurons and their projections, while striatal target neurons remain intact. The aSyn-induced neurotoxicity was also accompanied by neuroinflammation, a classic hallmark of PD and other neurodegenerative diseases, evidenced by increased staining for activated microglia (Iba-1 marker) and the infiltration of endogenous mouse immunoglobulins (IgGs; Figure 3C), the latter likely resulting from blood-brain barrier disruption.[23] Increased levels of IgG-light chains in AAV:aSyn-injected SN versus non-injected and AAV:GFP controls were also observed by western blot (Figure S1). Notably, our AAV:GFP injections are well tolerated and provide a key control for potential adverse effects related to general protein overexpression, since prior studies have observed neurotoxic effects caused by excessive AAV-mediated GFP expression in TH neurons.[24] Taken together, these data indicate that our AAV:aSyn model induces a consistent, time-dependent degeneration of TH^+ neuronal projections and cell bodies and neuroinflammation, providing a useful model to assess the effects of miR-181 modulation on these PD outcomes.

Effects of miR-181 overexpression on aSyn-induced neurotoxicity in mouse brain

Prior independent reports indicate that the miR-181a levels are increased in aged and PD human brain tissues, and our further interrogation of available datasets indicate that miR-181 target genes are coincidentally downregulated (Figure 1); however, the biological effects of elevated miR-181 levels on DA neuronal health and aSyn-induced PD outcomes were unknown. To begin addressing this, we evaluated the effects of elevated miR-181a/b in neurons in mice injected unilaterally with AAV:miR-181 (1.65×10^{10} vg) into the SN. At 18 weeks post-injection, TH staining was reduced in AAV:miR-181-treated hemispheres (Figure S3), indicating neurotoxic effects of excess miR-181 alone. To verify the specificity of miR-181 neurotoxicity, additional mice were injected unilaterally with 1.65×10^{10} vg of either AAV:miR-181 or AAV:U6-Ctrl, which expresses a scrambled miR control. After 9 weeks, AAV:miR-181 treatment led to ~65% reduced striatal TH staining intensity ($p < 0.001$) and ~45% loss of SN dopaminergic neurons ($p < 0.001$), relative to non-injected control sides; by contrast, TH staining was preserved in the AAV:U6-Ctrl group (Figures 4A–4C). Based on these observations, we hypothesized that elevated miR-181 may promote PD progression, and in the setting of aSyn overexpression, it would cause enhanced neurotoxicity. To address this hypothesis, we performed co-injections of AAV:aSyn plus AAV:miR-181, with dosing adjusted to test miR-181-mediated exacerbation. We used a lower dose of AAV:aSyn to elicit intermediate TH loss (2.5×10^9 vg), and we also lowered the amount of miR-181 vector to a non-toxic dose (2.5×10^9 vg). At 16 weeks post-injection, AAV:aSyn alone caused moderate DA neuron loss, based on striatal TH staining intensity as well as nigral TH^+ neuronal counts (injected versus non-injected; Figures 4D–4F). In comparison, the co-injection of AAV:aSyn and AAV:miR-181 elicited a striking exacerbation of TH loss; striatal TH staining was severely reduced (~80% decline, $p < 0.05$) in injected hemispheres, and ~60% of TH^+ neurons were lost in the pars compacta of the SN (SNpc; $p < 0.0001$). AAV:miR-181 alone at this same dose had no effect on either of these readouts, similar to buffer-injected and AAV:GFP-injected controls. Together, these findings support the notion that miR-181 overexpression is sufficient to induce neurotoxicity in dopaminergic neurons and can synergize with aSyn to further provoke neurotoxic outcomes in PD.

Effects of miR-181 inhibition on aSyn-induced neurotoxicity in mouse brain

Considering that miR-181a is elevated in human PD brains and that increased miR-181 exacerbated aSyn-induced neurotoxicity in the mouse brain, we hypothesized that blocking endogenous miR-181 may provide neuroprotection in the setting of aSyn overexpression. To address this, we tested the effects of AAV:TuD-181 treatment alone following direct injection into mouse SN. At 18 weeks post-injection, AAV:TuD-181-injected (2×10^{10} vg) and non-injected hemispheres were indistinguishable by TH staining, supporting the idea that prolonged TuD-181 RNA expression and miR-181 inhibition is well tolerated in DA neurons (Figure S4). We next conducted a co-injection study with AAV:aSyn (1.3×10^{10} vg) plus either AAV:TuD-181 or AAV:U6-Ctrl (1×10^{10} vg). In addition, AAV:GFP (1.3×10^{10} vg) plus AAV:U6-Ctrl (1×10^{10} vg) served as a control for potential artifacts related to protein and non-coding RNA overexpression. All of the injections were done bilaterally into the SN to allow the assessment of motor deficits. Accelerated rotarod and open-field ambulatory measures were collected from 15 to 20 weeks post-injection. However, AAV:aSyn + AAV:U6-Ctrl mice did not exhibit any robust and reproducible deficits in motor behavior compared to the control groups (AAV:aGFP + AAV:U6-Ctrl or non-injected mice, data not shown), precluding the ability to determine the significant influence of miR-181 manipulation on motor phenotypes in this model. Histological analyses performed at 24 weeks post-injection showed that mice treated with AAVs:aSyn + U6-Ctrl exhibited a marked reduction in striatal TH staining intensity relative

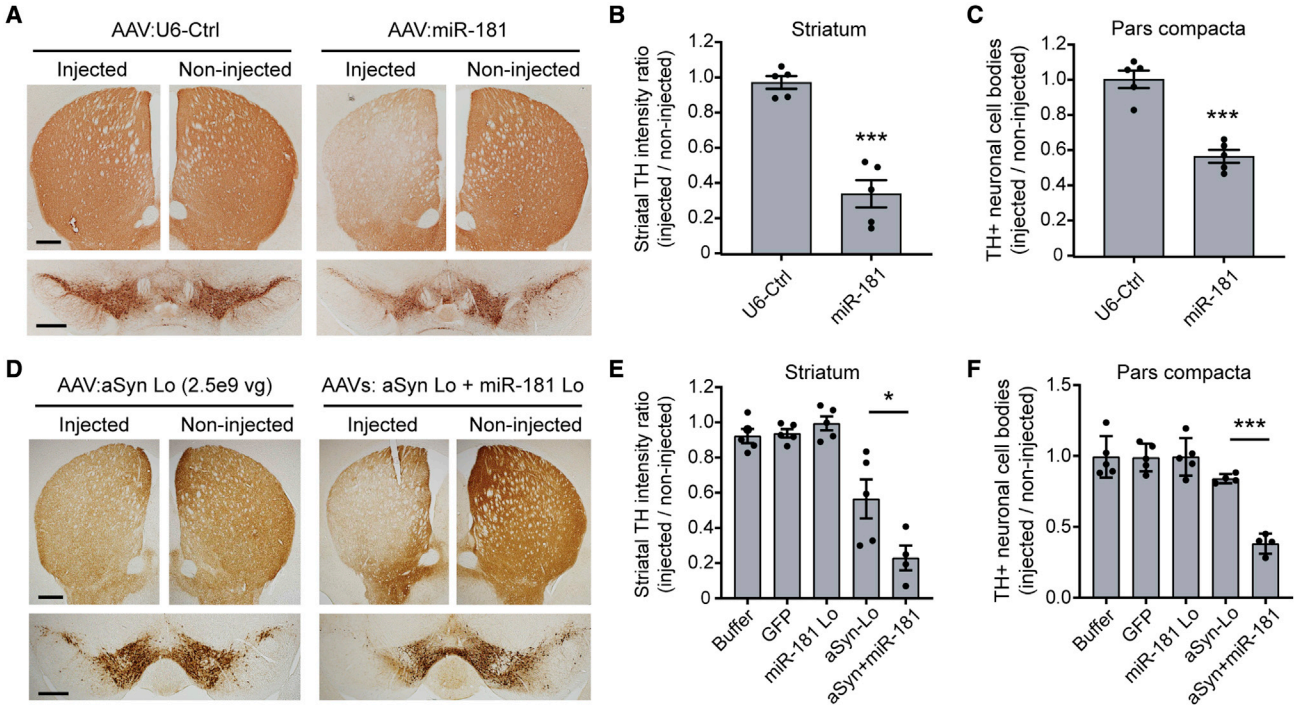

Figure 4. miR-181 overexpression induces TH$^+$ neuron degeneration and exacerbates aSyn-induced neurotoxicity

Histological analyses done on mouse brains injected unilaterally with AAV:U6-Ctrl (scrambled miR) or AAV:miR-181 (1.65×10^{10} vg; harvested at 9 weeks post-injection (A–C) or co-injected unilaterally with AAV:aSyn plus or minus AAV:miR-181 (each at a low of 2.5×10^9 vg; harvested at 16 weeks post-injection (D–F) into the SN. Buffer-injected and AAV:GFP-injected (1×10^{10} vg) were included as controls alongside the latter cohort. (A and D) Representative photomicrographs of immunohistochemical staining for TH$^+$ DA neurons in striatal and SN regions are shown. Image analyses were performed to quantify striatal TH staining intensity (B and D) and TH$^+$ neuronal cell bodies in the SNpc (C and F) in injected and contralateral non-injected control sides. Plotted data are represented as the means ± SEMs (n = 4–5/group); p values were obtained using either unpaired 2-tailed t tests (B and C) or 1-way ANOVA with Tukey's multiple comparisons test (E and F); ***$p < 0.001$ and *$p < 0.05$. Scale bars: 500 μm. Related to Figure S3.

to AAV:GFP control injected mice (∼50% decline, $p < 0.0001$; Figures 5A and 5B), consistent with our previous observations with unilateral injections of AAV:aSyn (Figures 3C and 3D). AAVs:aSyn + U6-Ctrl injection also resulted in the significant loss of TH$^+$ neuronal cell bodies in the SN SNpc (∼30% decline, $p = 0.01$; Figure 5C). By contrast, mice injected with AAVs:aSyn + TuD-181 showed remarkable protection against aSyn-induced neurotoxicity, as evidenced by the minimal (∼15%) loss of striatal TH staining and clear preservation in the numbers of TH$^+$ neurons in the SNpc (only an ∼5% decline). Relative to control AAVs:aSyn + U6-Ctrl mice, this protection was significant ($p = 0.01$ and $p < 0.05$ for striatal and SN TH$^+$ staining, respectively; Figures 5A–5C). This protection was not associated with lower aSyn transgene expression, as levels of human aSyn were similar in SN regions of AAVs:aSyn + U6-Ctrl and AAVs:aSyn + TuD-181 injected mice (Figure 5D). To assess the reproducibility of this TuD-181-mediated protective effect, we performed unilateral injections of either AAVs:aSyn + U6-Ctrl or AAVs:aSyn + TuD-181 and determined the striatal TH staining intensities (injected relative to non-injected hemispheres) 16 weeks later. Consistent with our prior results, the TH loss was significantly less severe in the AAVs:aSyn + TuD-181 treatment group compared to the AAVs:aSyn + U6-Ctrl injected group ($p < 0.01$; Figures 5E and 5F), further supporting the notion that the blockade of endogenous miR-181 protects against aSyn-induced neurotoxicity.

MiR-181 suppresses a diverse set of PD-related gene targets

To gain mechanistic insight into how miR-181 may influence neuronal function and viability in the SN, we performed mRNA-sequencing (mRNA-seq) on SN RNA samples collected from mice injected unilaterally with AAV:miR-181 to evaluate gene expression changes relative to non-injected contralateral control sides, while comparing the resulting data to mice injected unilaterally with AAV:GFP control virus to account for changes simply resulting from direct AAV injection. Differential expression analyses were conducted, yielding many significantly altered genes across treatment groups, with an obvious broad downregulation of miR-181 targets in mice injected with AAV:miR-181 (Figure 6A), which was not observed with AAV:GFP injection (Figure 6B). Also, many significantly upregulated genes were found in injected compared with non-injected hemispheres, likely due to an inflammatory response related to direct AAV injection; notably, this was more pronounced in AAV:miR-181 samples versus AAV:GFP samples. An unbiased

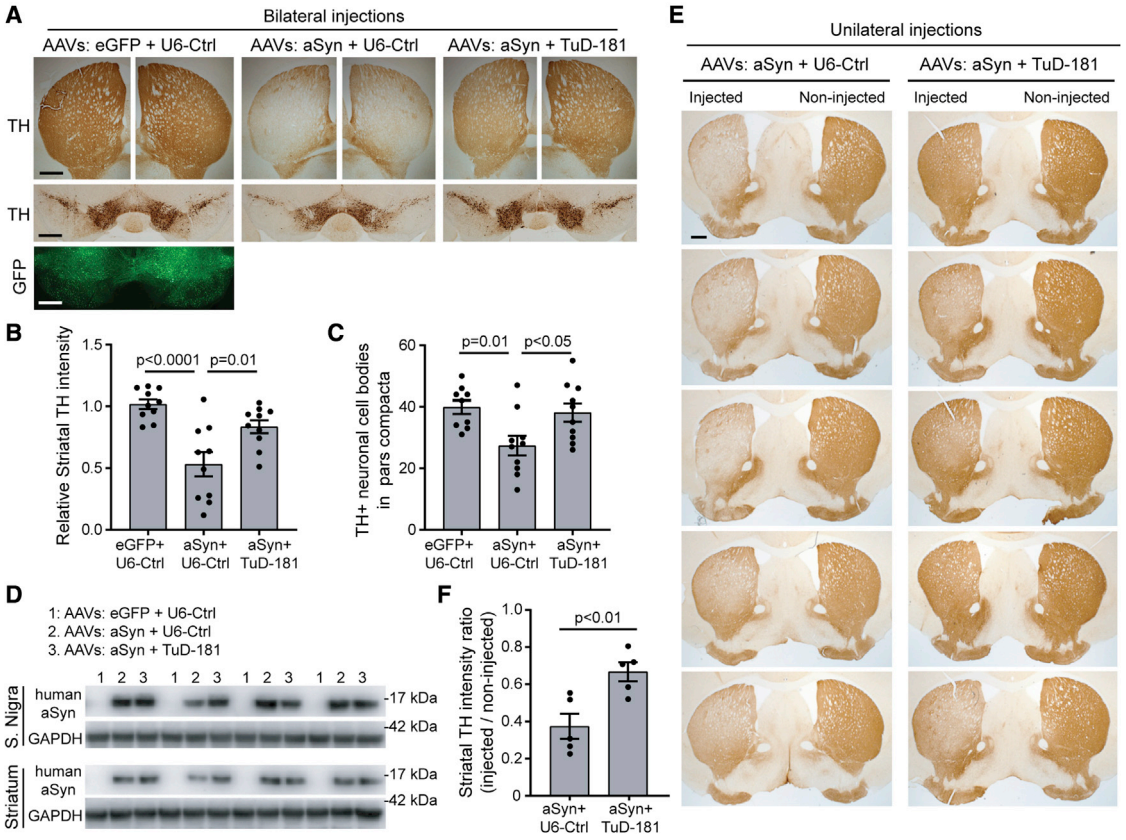

Figure 5. TuD-181 protects against aSyn-induced neurotoxicity

Histological (A–C) and western blot (D) analyses done on mouse brains harvested 24 weeks after bilateral stereotaxic co-injection with either AAV:GFP or AAV:aSyn (each at 1.3×10^{10} vg) in combination with either AAV:U6-Ctrl, which expresses a scrambled stem-loop RNA control or AAV:TuD-181 (each at 1×10^{10} vg). (A) Representative photomicrographs of native GFP fluorescence or immunohistochemical staining for TH^+ DA neuronal cell projections and cell bodies in striatum (top) and SN (below), respectively. Image analyses were performed to quantify striatal TH staining intensity (B) and TH^+ neuronal cell bodies in the SNpc (C). The plotted data are represented as the means ± SEMs (n = 9–10/group); the p values comparing the indicated groups were obtained using 1-way ANOVA with Tukey's multiple comparisons test. The data indicate that TuD-181 significantly reduces the extent of neurodegeneration and neuronal cell loss induced by AAV:aSyn. (D) Western blot analyses were performed to determine whether TuD-181 influences the expression of human aSyn transgene in SN or striatal tissues; no significant effect was observed (n = 4/group). (E and F) Histological analyses done on mouse brains harvested 16 weeks after unilateral stereotaxic co-injection of AAV:aSyn (1.3×10^{10} vg) in combination with either AAV:U6-Ctrl, which expresses a scrambled stem-loop RNA control, or AAV:TuD-181 (each at 1×10^{10} vg). Representative photomicrographs of immunohistochemical staining for TH^+ DA neuronal cell projections in the striatum are shown for each mouse (n = 5/group). Image analyses were performed to quantify striatal TH staining intensity, and ratiometric data (injected versus non-injected hemisphere) plotted in the bar graph, represented as the means ± SEMs. The p value comparing the 2 groups was obtained by 2-tailed unpaired t test. Scale bars: 500 μm. Related to Figure S4.

query of heptamer motif frequencies in mRNAs revealed that heptamers corresponding to miR-181 seed sequences were the most significantly enriched heptamers among the downregulated mRNAs (across both coding and 3′-untranslated regions [3′UTRs]) in miR-181 overexpression mice (Figure 6C). In addition, cumulative distribution analyses confirmed that miR-181 mRNA targets are overall significantly shifted toward lower expression levels (Figure 6D). Taken together, these findings provide strong support that our neuron-targeted AAV-mediated miR-181 overexpression strategy robustly induces the expected downregulation of a diverse set of miR-181 target mRNAs. Gene set enrichment analyses (using ToppFun, ToppGene Suite[25]) performed on genes that were significantly downregulated in AAV:miR-181 samples ($p < 0.05$), but not in AAV:GFP samples ($p > 0.2$), indicated that miR-181 overexpression broadly coordinated the repression of genes involved in synaptic signaling, neurite and axonal projection, ion transport, mitochondrial metabolism/respiration, and calcium signaling (Figure 6E).

Beyond the downregulated genes, we found that genes showing significant increases in expression following AAV:miR-181 treatment ($p < 0.05$), but not increased with AAV:GFP ($p > 0.2$), were enriched for immune system pathways (e.g., leukocyte activation, positive regulation of nuclear factor κB (NF-κB), cytokine, and Toll-like receptor 4 [TLR4] signaling), suggesting that the neuronal overexpression of miR-181 may trigger neuroinflammatory responses above and beyond that caused merely by direct AAV injection. These findings

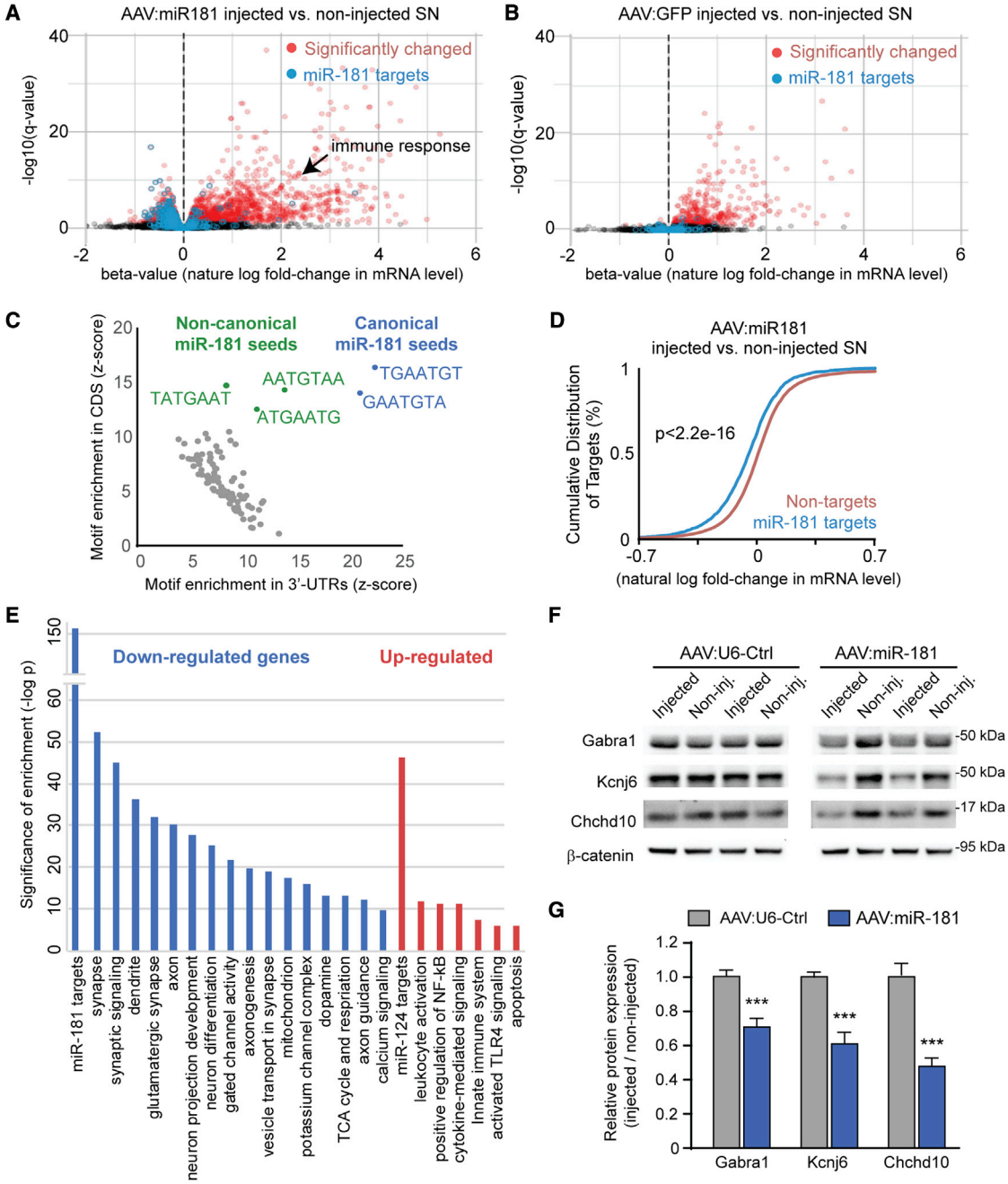

Figure 6. Characterization of miR-181 targets in mouse SN

mRNA sequencing was performed on SN RNA samples collected from mice 3 weeks after unilateral injection with AAV:miR-181 or AAV:GFP into the SN, and differential gene expression analyses were done to compare injected versus contralateral non-injected control hemispheres. (A and B) Volcano plots are shown with significant changes defined as $q < 0.05$. (C) Plot showing the most significantly enriched heptamer sequences in downregulated mRNAs (in both 3′UTR and coding sequences [CDSs]), based on cWords algorithm *Z* scores. Sequences complementary to miR-181 are highlighted in green and blue. (D) Cumulative fraction analysis of the gene expression data show that mRNA levels of miR-181 target genes (blue) are broadly downregulated (i.e., leftward shifted), relative to non-target genes, red) in AAV:miR-181 injected versus non-injected hemispheres. Kolmogorov-Smirnov (KS) test p values are provided. (E) Gene Ontology analyses performed on genes that were significantly down- or upregulated after AAV:miR-181 treatment ($p < 0.05$), but not changed in AAV:GFP samples ($p > 0.2$). (F and G) Western blot analyses were performed using SN protein lysates harvested from mice 3 weeks after unilateral injection with either AAV:miR-181 or AAV:U6-Ctrl (scrambled miR control) to assess whether select miR-181 target genes were also down-regulated at the protein level. Densitometry analysis was performed to quantify the expression levels, normalized to beta-catenin loading controls. The data are represented as the means ± SEMs (n = 5/group), and the p values were obtained by 2-tailed unpaired t tests. Related to Figure S5.

were further supported in subsequent western blot analyses, which revealed an abundance of mouse IgG-light chains in AAV:miR-181-treated SN lysates (Figure S5), similar to those observed with AAV:aSyn treatment (Figure S1); by contrast, IgG-light chains were only weakly detected in AAV:GFP-injected brains (Figure S5).

We next chose select targets from our mRNA-seq results to validate miR-181-mediated target suppression at the protein level. We focused on targets with miR-181 binding sites (computationally predicted and/or miR-181 sites physically bound by Ago2-RISC complexes in human and mouse tissues, including brain,[11,15,20,26] and further narrowed selection based on the following: (1) expression in SN neurons, (2) relevance to DA neuronal function, and (3) availability of antibodies. Three genes that met these criteria were *Gabra1*, *Kcnj6*, and *Chchd10*, and these represent various types of miR-181 binding sites (e.g., a canonical Gabra1 3′UTR site found by TargetScan prediction and Ago2-pulldown, a *Kcnj6* 3′UTR site missed by TargetScan due to poor 3′UTR annotation but found by Ago2-pulldown, a non-canonical *Chchd10* 3′UTR found by Ago2-pulldown). *Gabra1* encodes the alpha 1 subunit of GABAA inhibitory neurotransmitter receptors, which are critical to the basal ganglia-SN circuitry regulating dopamine-driven movement.[27] *Kcnj6* encodes Girk2, a G protein-activated potassium channel that provides negative feedback to limit neuronal firing and dopamine release.[28] *Chchd10* encodes a coiled-coil-helix-coiled-coil-helix domain containing protein that partners with Chchd2 to support mitochondrial cristae maintenance and respiratory function.[29] Notably, mutations in *Chchd10* and *Chchd2* have been linked to frontotemporal dementia and amyotrophic lateral sclerosis (ALS) and PD, respectively.[30,31] Initial western blotting of protein lysates collected from mice used for the mRNA-seq study showed trends toward reduced levels of Gabra1, Kcnj6, and Chchd10 proteins, respectively, in AAV-miR-181-injected SN relative to non-injected SN ($p < 0.1$), but no significant change after AAV-GFP injection ($n = 3–5$/group; Figure S5). To increase sample numbers and include a more appropriate control group, additional mice were injected unilaterally with 1.65×10^{10} vg of either AAV:miR-181 or AAV:U6-Ctrl, which expresses a scrambled miR control. Western blotting of SN samples collected from these mice at 3 weeks post-injection showed significantly decreased (30%–50%) Gabra1, Kcnj6, and Chchd10 protein levels in AAV-miR-181-injected SN relative to non-injected control sides ($p < 0.001$), while AAV:U6-Ctrl mice showed no unilateral differences in the expression of these proteins (Figures 6F and 6G). Together, these data demonstrate that miR-181 functionally suppresses mRNA levels for hundreds of gene targets with diverse functions and potential relevance to PD pathogenesis and provide general support that the observed mRNA decreases are also reflected at the protein level.

DISCUSSION

This study began with an interest in the potential relevance of increased miR-181 levels in PD patient samples.[6,7] We now show that elevated miR-181 coincides with broad decreases in miR-181 target gene mRNAs in both aged and PD brain samples collected from human patients and rodent models. Our analyses indicate a trend toward larger decreases in miR-181 target gene mRNAs in aged versus young compared to PD versus control samples, suggesting that natural aging more profoundly enhances miR-181 functions and that this may contribute to provoking PD onset and progression with advanced age. One important limitation worth noting is that these public data lack information on actual miR-181 levels in each of the samples, and thus these analyses are only capable of correlatively, not directly, linking the prior separately published observations of miR-181 elevations in PD and aging brains to broad decreases in miR-181 target gene expressions, as we show in Figure 1. To understand whether miR-181 augments or antagonizes PD, we manipulated miR-181 levels in the context of a PD mouse model, elicited by AAV5 vector-mediated overexpression of human aSyn in the SN. Collectively, our findings indicate that elevated miR-181 exacerbates, while blockade of endogenous miR-181 diminishes, neuronal loss incurred by aSyn overexpression.

For our AAV-based PD model, we chose the serotype 5 capsid, previously demonstrated to transduce mouse DA neurons,[32] with the aSyn transgene cassette incorporating the neuronal specific synapsin-I promoter plus WPRE (post-transcriptional regulatory element of woodchuck hepatitis virus) elements, shown by others to enhance SNpc loss and disease severity.[4,32] At 3 weeks post-injection into the SN (1×10^{10} vg dose), we achieved an approximate 4-fold overexpression of aSyn, which triggered pathogenic events that led to the significant loss of TH staining by 9 weeks. Our model is consistent with similar AAV-generated rodent models,[33–35] displaying salient features of PD, including neuroinflammatory responses (IgG influx and reactive Iba^+ microglia), enhanced phosphorylated aSyn (P-S129), and progressive loss of TH^+ striatal projections and DA SNc neurons. Although we were unable to reliably detect significant deficits in rotarod performance or open field ambulatory parameters, this was not surprising since PD-related motor dysfunction typically does not manifest unless SNpc neuron loss exceeds approximately 60%,[33] a level that was not consistently reached in our studies. Nevertheless, our model displayed characteristic pathological PD features, with a significant loss of TH^+ projections/neurons, indicative of SNpc DA dysfunction, degeneration, and death, providing indicators of disease severity to gauge the effects of miR-181 modulation.

Interestingly, we found that ~4-fold overexpression of miR-181a/b alone was toxic to DA neurons, which is compatible with reports implicating miR-181 in provoking cell death in stroke, seizure, or mitochondrial disease models.[18,19,36] When delivered at a lower non-toxic dose and co-injected with AAV:aSyn, AAV:miR-181 markedly exacerbated the extent of aSyn-induced striatal TH loss, making it worse, from ~45% to ~80%. This leads us to speculate that aging-related increases in miR-181 levels could hasten the onset and progression of PD in patients. Conversely, we found that co-injection of AAV:TuD-181 with AAV:aSyn had the opposite effect, protecting against aSyn-induced neuronal toxicity (50%–65% versus 15%–30% striatal TH loss), supporting the need to further explore the therapeutic potential of miR-181 inhibition in the setting of PD. Beyond our gene therapy approach, this is supported by additional studies, which

demonstrated neuroprotection in mice with the genetic reduction of miR-181 expression, achieved by partial knockout strategies.[18]

Despite several studies supporting the idea that miR-181 may promote neuronal dysfunction and death, the mechanisms by which this occurs remain unclear due to the lack of comprehensive empirical data for miR-181 functional targeting. Here, we describe the first transcriptome-wide gene expression dataset characterizing the effects of miR-181 overexpression in rodent brains. This dataset reveals that miR-181 operates by suppressing a diverse set of gene targets, 282 of which harbor cross-species conserved miR-181 sites predicted by TargetScan. While others have attributed the neuroprotective effects of miR-181 inhibition to its regulation of genes that block apoptosis or influence mitochondrial function and biogenesis,[18,19,36] our dataset points to an even broader effect, with many miR-181 gene targets operative in synaptic signaling, axon growth/stability, ion transport, calcium signaling, and mitochondrial function, all of which likely contribute to shaping the course of PD. For example, several notable downregulated miR-181 targets include genes that are protective in PD model systems (e.g., *Kcnh1*, *Slc2a3*, *Atg5*, *Nrg1*)[37–40] or play important roles in establishing or maintaining the DA neuronal cell phenotype (e.g., *Rspo2*, *Bmp2*).[41,42] In addition, our mRNA-seq data support the notion that AAV:miR-181 injection, relative to AAV:GFP controls, results in enhanced immune activation and increased expression of miR-124 target genes, hinting at possible miR-181-mediated miR-124 inhibition by unknown mechanisms. The latter is noteworthy since prior reports indicate that miR-124 protects against neurodegeneration, including studies in PD models.[43]

Given that miRs are known to coordinate biological responses through targeting multiple genes within a shared pathway, it is conceivable that in a disease setting, miR-181 regulates a defined subset of genes that sway neurons to their demise. Such a gene set may be unique to PD or extend to other synucleinopathies (e.g., dementia with Lewy bodies) or even more broadly to neurodegenerative disease/neuropathy. While our mRNA-seq data provide a great resource to better understand miR-181 functions in the brain, it represents a snapshot of gene expression at 3 weeks post-miR-181 overexpression. To better discern potential mechanisms related to the therapeutic manipulation of miR-181, a more comprehensive mRNA-seq study is needed to further define miR-181 target gene fluctuations in the setting of and through the course of PD. Nevertheless, the current dataset can be further queried for additional miR-181 target interactions related to PD and beyond. For example, miR-181 has been implicated in stroke-induced neuronal death and was found to be upregulated in response to cocaine, having potential involvement in cocaine addiction. Notably, our gene enrichment analyses (via ToppFun) identified cocaine as the top hit in the drug category, indicating an alignment of cocaine-related genes and our miR-181 downregulated gene set in the mouse brain.

In summary, our new data are compelling and suggest that miR-181 upregulation provokes DA neuronal cell death and accelerates aSyn-induced neurotoxicity, thus warranting future studies to delineate the underlying mechanisms and better characterize pathways that lead to elevations in miR-181 expression in DA neurons. With respect to the latter, it is interesting to note that several pesticides previously linked to the risk of PD manifestation have been shown to elicit robust increases (~3- to 4-fold) in miR-181 levels in various experimental settings.[44–46] The potential translational significance of these independent observations along with our findings are worthy of further investigation. Finally, follow-up studies are needed to further advance pre-clinical testing of miR-181 inhibition as a therapeutic strategy for PD. One notable limitation to this present work is that we were unable to examine the potential impact of miR-181 modulation on PD-related motor phenotypes since our model served primarily as a model of aSyn-induced DA neuronal loss and did not consistently reach the loss threshold (>60%) at which behavioral deficits are reliably detected. While our data support that miR-181 inhibition in mouse SN is well tolerated, moving forward, it will be critical to thoroughly assess the effects of miR-181 modulation on motor phenotypes in other PD models (and species) with more robust behavioral deficits to better understand the potential clinical relevance. Given our promising results with viral-based miR inhibition, follow-up pre-clinical studies should also include the testing of synthetic anti-miR oligonucleotides, which can be more readily dosed and withdrawn as needed.

MATERIALS AND METHODS

Plasmids

To create the miR-181 target reporter plasmid, a synthetic DNA oligo with the sequence 5′-CTCGAGGTGAATGTTACCTTGAAATGCT CCAACCTGAATGTTAGGTTTGCCGTTGAATGTTAGCGGCCG C-3′ containing 3 miR-181 binding sites (IDT, Coralville, IA) was introduced downstream of the Renilla luciferase expression cassette (using XhoI and NotI restriction enzyme sites) in the psiCheck2 dual luciferase plasmid (Promega, Madison, WI). pAAV2/5-U6:TuD-Ctrl (TuD-Ctrl) and pAAV2/5-U6:TuD-181 (TuD-181) shuttle plasmids were constructed by inserting DNA oligo sequences (IDT) to express the following TuD stem-loop sequences from the U6 promoter: GACGGCCTCGAGACTGGAACCTACACAATG CAGAAATACCACAAGTATTCTGGTCACAGAATACAACCAT CACAATGCAGAATAACCACAACTAGTCTCGGGGCCGTCTTT for TuD-Ctrl, and GACGGCCTCGAGACTGGCAACTCACCGA CAAAGATGAATGTTCAAGTATTCTGGTCACAGAATACAAC CTTACCGACAAAGATGAATGTTAACACTAGTCTCGGGGCC GTCTT for TuD-181, both cloned into a custom version of pFBAAV-mU6mcsCMVeGFPSV40pA (ID no. G0347, University of Iowa Viral Vector Core Facility, Iowa City, IA [UIOWA VVC]). CMVmiR-181a1b2 plasmid was constructed by ligating a custom gBLOCK DNA fragment containing tandem miR-181a1 and miR-181b2 sequences (~450–500 bp of human genomic sequence centered on each miR loop) into pFBAAVCMVmcspBgHpA (ID no. G0347 UIOWA VVC). CMV-SNCA plasmid was created by the blunt ligation of a synthetic DNA gBLOCK (IDT) of human SNCA cDNA with flanking restrictions sites (SpeI-BglII-SNCA-MfeI-SpeI) into pCR-Blunt-II-TOPO (Thermo Fisher Scientific, Waltham, MA)

followed by the digest of TOPO-SNCA with SpeI and ligation into NheI-digested pFBAAVCMVmcspBgHpA (ID no. G0347 UIOWA VVC). To create the pAAV2/5-hSYN1-SNCA shuttle plasmid, an AAV shuttle plasmid with the human synapsin-1 promoter and a WPRE (plasmid no. 50465 Addgene, Watertown, MA) was digested with BamHI and EcoRI, dropping out the EGFP. The SpeI-BglII-SNCA-MfeI-SpeI gBLOCK was digested with BglII and MfeI and ligated into the AAV shuttle, replacing the EGFP. To create the pAAV2/5-hSYN1-miR-181a1b2 shuttle plasmid, standard cloning techniques were used to remove EGFP from the parental shuttle plasmid (Plasmid no. 50465 Addgene) and replace it with the gBLOCK DNA fragment containing tandem miR-181a1 and miR-181b2 sequences.

AAV2/5 vectors

All AAV vectors were prepared at the UIOWA VVC and contain vector genomes flanked by AAV2-type inverted terminal repeats (ITRs), packaged into AAV serotype 5 capsids, by standard triple transfection (3XT) or baculovirus (BAC) methods. AAV2/5hSynEGFP (AAV:GFP; 3XT) and AAV2/5mU6-miSafeCMVeGFP (AAV:U6-Ctrl; BAC) were purchased as in-stock vectors from UIOWA VVC (catalog nos. VVC-U of Iowa-3412 and VVC-U of Iowa-258). Shuttle plasmids pAAV2/5-U6:TuD-181, pAAV2/5-hSYN1-miR-181a1b2, and pAAV2/5-hSYN1-SNCA described above) were supplied to the UIOWA VVC to generate custom AAV preparations of AAV:TuD-181 (BAC), AAV:miR-181 (3XT), and AAV:aSyn (3XT), respectively. AAV purification was done with an iodixanol gradient followed by ion exchange using MustangQ Acrodisc membranes (Pall, East Hills, NY), and titers of purified AAV preparations (vector genomes per ml, vg/mL) were determined by qPCR.

Test of TuD181 construct in N2A cells

Mouse Neuro2a (N2a) cells (CCL-131, American Type Culture Collection [ATCC], Manassas, VA) were seeded at 80,000 cells/well in 24-well tissue culture dishes, and the next day, cells were co-transfected with 100 ng miR-181 target reporter plasmid plus 4 nM either control or miR-181 pre-miR synthetic oligos (Ambion, Austin, TX), along with 100 ng either TuD-Ctrl plasmid or TuD-181 expression plasmid, using Lipofectamine 2000 (Thermo Fisher Scientific). Each combination was assayed in triplicate culture wells. At 48 h post-transfection Firefly (FF) and Renilla (R) luciferase activities were measured using the GloMax Microplate Reader and Dual Luciferase Kit reagents (Promega). Briefly, culture media was removed and 200 μL passive lysis buffer was added to each well. The plate was incubated on a shaker for 15 min at room temperature, and then 10-μL lysate was transferred to duplicate wells of a 96-well white plate. Luminescence from FF and R was determined from 5-s reads after the injection of respective substrates to each well. The R:FF ratio was calculated and adjusted relative to the control (set to "1"), and results are expressed as the mean ± SEM (n = 4/group).

Test of CMVmiR-181a1b2 construct in HEK293

HEK293 cells (CRL-1573 ATCC) were seeded at 100,000 cells/well in 24-well plates and transfected 24 h later for use in either luciferase assay or qRT-PCR. For the luciferase assay, cells were co-transfected with 20 ng of the miR-181 target reporter plasmid and 200 ng of either control parental plasmid (CMV only) or CMVmiR-181a1b2, using Lipofectamine 2000. At 48 h post-transfection, lysates were collected from cultures and transferred to duplicate wells for luminescence readings. Luminescence from FF and R was determined from 5-s reads after the injection of the respective substrates. The R:FF ratio was calculated and adjusted relative to the control (set to "1"), and the results are expressed as the mean ± SEM (n = 3 for CMV-only control; n = 6 for CMVmiR-181a1b2.

Stereotaxic injections

Experiments with mice were performed in accordance with University of Iowa Animal Care and Use Committee (IACUC) regulations. C57Bl/6J mice were purchased from JAX (stock no. 000664, JAX, Bar Harbor, ME) and housed under a 12/12-h light/dark cycle with access to food and water *ad libitum*. Stereotaxic injections were performed on female C57BL/6J mice at 8–11 weeks of age. Under anesthesia, the head was shaved and treated with antiseptic and the mouse placed in a stereotactic head frame (Stoelting, Wood Dale, IL). A midline incision was made in the scalp and a small burr hole was drilled at the appropriate coordinates. Using a 33-G blunt needle on a 5-μL Neuros Syringe (Hamilton, Reno, NV), 1.5 μL vector was injected at a rate of 0.2 μL/min, at coordinates anteroposterior (AP) 3.2 mm, mediolateral (ML) 1.3 mm, and dorsoventral (DV) 4.2 mm from the dura to target the SN region.[47] The needle was left in place for an additional 5 min before slowly withdrawing over 2 min. For 6-OHDA injections, 6-OHDA (6-hydroxydopamine hydrobromide, Sigma-Aldrich, St. Louis, MO) was dissolved at 1 mg/mL (free base concentration) in 0.9% saline with 0.03% acetic acid, made fresh before use. Using stereotaxic injection procedures as described above, 1 μL was injected in the medial forebrain bundle at coordinates AP 1.2 mm, ML 1.2 mm, and DV 4.75 mm from the dura. the control mice received 0.03% acetic acid in a 0.9% saline injection. 6-OHDA-injected and control mice received a pre-surgery intraperitoneal (i.p.) injection of 25 mg/kg desipramine HCl (Sigma-Aldrich), dissolved in saline, to protect the noradrenergic neurons. All of the mice were given 1.0 mL lactated Ringers subcutaneously (s.c.) to provide hydration during surgical recovery.

Antibodies and stains

Antibody and dilutions were as follows: TH (AB152 rabbit polyclonal IgG, MilliporeSigma, Burlington, MA) 1/1,000 for staining tissue sections and 1/3,500 for western blot; aSyn (sc-58480 mouse IgG1 clone LB509, specific for humans; SCBT, Dallas, TX) 1/500 for staining tissue sections and 1/1,000 for western blot; phospho S129 aSyn (ab51253 rabbit monoclonal IgG, Abcam, Cambridge, MA) 1/1,000 for staining tissue sections and 1/3,000 for western blot; aSyn (BD 610786 mouse IgG, clone 42, reacts with human and mouse, BD Biosciences, San Jose, CA) 1/1,000 (0.25 μg/mL final) for western blot; glyceraldehyde 3-phosphate dehydrogenase (Gapdh) (AC002 mouse IgG, Abclonal, Woburn, MA) 1/30,000 for western blot; beta catenin (PLA0230 rabbit polyclonal, Sigma-Aldrich) at 1/3,000 for western blot; Iba1 (019–19,741 rabbit polyclonal, Fujifilm Wako Chemicals,

Richmond, VA) 1/5,000 for staining tissue sections; dopamine transporter (MAB369 rat monoclonal IgG clone DAT-Nt, Sigma-Aldrich) at 1/2,000 for staining tissue sections; Darpp-32 (MAB4230 rat monoclonal IgG clone no. 375604, R&D Systems, Minneapolis, MN) at 1/500 (0.5 μg/mL) for staining tissue sections; GFP (A-6455 rabbit IgG, Thermo Fisher Scientific) $^{1}/_{2}$,500 for tissue staining; beta-actin (A5441 mouse monoclonal antibody [mAb] IgG clone AC-15 ascites, Sigma-Aldrich) 1/20,000 for western blot; Chchd10 (25671-1-AP, rabbit polyclonal antibody, Proteintech, Rosemont, IL) at 1/750 (0.4 μg/mL) for western blot; Gabra1 (12410-1-AP, rabbit polyclonal antibody, Proteintech) at 1/2,000 (0.1 μg/mL) for western blot; Girk2/Kcnj6 (21647-1-AP, rabbit polyclonal antibody, Proteintech) at 1/1,000 (0.4 μg/mL) for western blot; horseradish peroxidase (HRP)-conjugated goat anti-mouse IgG (115-035-146, Jackson ImmunoResearch, West Grove, PA) 1/2,000 for staining tissue sections and 1/20,000 for western blot; HRP-conjugated goat anti-rabbit IgG (111-035-144, Jackson ImmunoResearch) 1/2,000 for staining tissue sections and 1/80,000 for western blot; HRP-conjugated goat anti-mouse IgG light chain (115-035-174, Jackson ImmunoResearch) 1/20,000 for western blot; HRP-conjugated goat anti-rat IgG (112-035-167, Jackson ImmunoResearch) 1/2,000 for staining tissue sections; Alexa Fluor conjugated goat anti-rabbit or goat anti-mouse IgG (Thermo Fisher Scientific) 1/2,000 for staining tissue sections. Alexa Fluor 488 conjugated wheat germ agglutinin (A488WGA) and ToPro 3 (Thermo Fisher Scientifc) were used at 1/1,000 for tissue section staining.

Tissue processing for RNA/protein analyses

For the collection of SN and striatal regions for RNA and/or protein analyses, brains were harvested from mice after isoflurane overdose and cervical dislocation and immediately submerged for 5 min in ice-cold PBS before collecting slices. The coronal brain matrix (Precision Brain Slicer, Braintree Scientific, Braintree, MA) and all of the instruments and single-edge razor blades were pre-cooled and kept on ice. Slices were collected caudal to rostral, with the first blade inserted just rostral to the cerebellum. After placement of the second blade in the next slot, the first blade, carrying a 1-mm coronal brain slice, was removed and placed tissue side up on an ice-cold block. This procedure of "next" blade placement and previous blade retrieval was continued rostrally through the brain. Regions of SN and striatum were dissected from the slices, snap-frozen in liquid nitrogen, and stored at −80°C until processing. Tissue pieces were homogenized in 150- to 200-μL ice-cold lysis buffer (50 mM Tris, 120 mM NaCl, 5 mM EDTA, 1% Triton X-100) with protease and phosphatase inhibitors (Sigma-Aldrich or Thermo Fisher Scientific) using disposable pellet pestles. For RNA isolation, approximately 75–100 μL lysate was transferred to 1 mL TRIzol (Thermo Fisher Scientific) and stored at −80°C until processing. To the remaining lysate, SDS and sodium deoxycholate detergents were added to the final 0.1% and 1%, respectively, and lysates were sonicated with a probe sonicator (2 rounds of 3 s, at a setting of 3) to reduce viscosity. Lysates were clarified by 10-min 4°C centrifugation at 10,000 × *g*, and supernatants were transferred to fresh tubes. Protein concentrations were determined by bicinchoninic acid (BCA) (Thermo Fisher Scientific) and equilibrated for all of the samples. Samples were resolved by denaturing electrophoresis on precast 4%–12% bis-tris gradient polyacrylamide gels using NuPage reagents (Thermo Fisher Scientific), and transferred to polyvinylidene fluoride (PVDF) using NuPage transfer buffer with 10% ethanol and 0.01% SDS. After transfer, the lower region of the PVDF membrane (for the detection of aSyn) was fixed in 0.8% paraformaldehyde (PFA) in PBS for 30 min.[48] All of the membranes were incubated for 1 h in a block solution of 5% dry milk dissolved in Tris-buffered saline with 0.1% Tween 20 (TBST), followed by primary antibody diluted in 2.5% dry milk in TBST overnight at 4°C. Blots were incubated for 1 h with HRP-conjugated secondary and developed by chemiluminescence on a VersaDoc Imaging System with Quantity-One software (Bio-Rad, Hercules, CA). Band intensities were normalized to a loading control band (beta-actin, GAPDH, or beta-catenin) in the same lane.

Test of SNCA construct for protein

Our sequence for human SNCA cDNA was tested *in vitro* for protein expression using the CMV-SNCA expression plasmid. HT1080 cells (CCL-121, ATCC) were seeded at 50,000 cells/well in 24-well plates and transfected 24 h later with 300 ng CMV-SNCA (in triplicate culture wells) using Lipofectamine 2000. At 48 h post-transfection, lysates were collected into 1% SDS with protease inhibitors (Roche, Indianapolis, IN), sonicated, and protein concentrations equilibrated. Samples were resolved by denaturing electrophoresis on precast polyacrylamide gels and western blot performed as described above, for the detection of aSyn (human plus mouse) and beta-actin as a loading control.

qRT-PCR

Total RNA was isolated from TRIzol according to the manufacturer's instructions (Thermo Fisher Scientific) and dissolved in TE (IDT) and quantified by nano-drop. RNA was DNase treated using a DNA-free kit (Thermo Fisher Scientific). Reverse transcriptase (RT) and qPCR reactions for miR were performed essentially according to the TacMan Small RNA Assays protocol using TaqMan MicroRNA Assays for 2-step qRT-PCR (hsa-miR-181a, ID no. 000480; hsa-miR-181b, ID no. 001098; hsa-miR-29a, ID no. 000412; snoRNA135, ID no. 001230) (Applied Biosystems, Thermo Fisher Scientific). Briefly, 15-μL RT reactions were set up containing 1× MultiScribe RT buffer, 2 mM deoxynucleotide triphosphate (dNTP) (0.5 mM each), 50 U Multiscribe, 3.8 U RNase inhibitor, 24 ng total RNA, and 1× concentrations of each TacMan assay RT primer in the pool, on ice. The pools for RT primers were miR-181a + miR-29a + snoRNA135 and miR-181b + miR-29a + snoRNA135. The thermocycler conditions for RT were 16°C for 30 min, 42°C for 30 min, 85°C for 5 min, and 4°C hold. After RT, cDNA samples were diluted 5-fold by the addition of nuclease-free water. For qPCR, 10-μL reactions were set up in TaqMan Universal Master Mix II with 4 μL diluted cDNA and a 1× concentration of appropriate TaqMan miR primer/probe set, in a 384-well plate in triplicate. qPCR reactions were performed on a ViiA™ 7 real-time PCR system with QuantStudio™ software (Thermo Fisher Scientific). Relative quantification (ΔΔCt) was used to analyze results, using

SnoRNA135 as the reference gene (endogenous control). For samples from unilateral injections, the results are expressed as the injected side relative to the non-injected side.

Immunostaining and image analyses

For brain histology, mice were perfused with 10 mL ice-cold PBS followed by 15 mL ice-cold 4% PFA in PBS, brains removed, post-fixed 24 h at 4°C, and then transferred to 30% sucrose in PBS at 4°C. After 2–3 days of completion of sinking in sucrose, brains were covered in Tissue-Tek O.C.T. Compound (EMS, Hatfield, PA) in Peel-a-Way embedding molds and frozen by setting molds in a dry ice/ethanol bath. Coronal 40-μm floating sections were cut on a cryostat and stored at −20°C in antifreeze medium (300 g sucrose, 300 mL ethylene glycol, to 1 L final volume with 0.1 M phosphate buffer, pH 7.4). Before staining, sections were washed for 10 min in PBS and endogenous peroxidase activity was quenched by a 20-min incubation in 1.5% H_2O_2 in PBS. Sections were washed in PBS then blocked/permeabilized by incubating for 2 h at room temperature in PBS containing 10% normal goat serum (NGS) and 0.3% Triton X-100, and then incubated overnight at room temperature with primary antibody diluted in PBS containing 0.1% Triton X-100 and 1% NGS (Ab diluent). Sections were washed 3 times for 15 min each in PBS before incubating with HRP-conjugated secondary antibody at 0.5–1 μg/mL in Ab diluent for 2 h at room temperature. Sections were washed twice in PBS and once in imidizole/acetate buffer (IAB) (10 mM imidazole, 83 mM sodium acetate, pH adjusted to 7.4 with glacial acetic acid) before developing in 3,4-diaminobenzoic acid (DAB) reagent (0.5 mg/mL DAB and 0.006% H_2O_2 in IAB) made fresh from stocks just before use. Care was taken to equilibrate the development times for sections across groups within the same experiments. Development was stopped by replacing DAB reagent with IAB, followed by transfer to PBS. Sections were floated in 20 mM Tris, pH 7.5, and mounted onto glass plus slides, dried overnight on the bench, then dehydrated through sequential 5-min incubations in 95%/100%/100% ethanol/zylene/zylene, then coverslipped with Tek-Select Clear Permaslip mounting medium (IMEB, San Marcos, CA). Bright-field images were captured on a BX53 upright scope with a DP72 camera and cellSens software (Olympus, Center Valley, PA). Capture settings were identical across slides within the same experiment. DAB staining intensities for TH-stained striatum were determined using ImageJ/Fiji. Briefly, the striatal region (caudate putamen) was outlined using the drawing tool and the mean intensity (range of 1–255) was measured and inverted (255 mean intensity). The background (from a non-stained region of the cortex) was subtracted. For bilateral experiments, intensities for each striatum are expressed relative to the non-injected control group (set to "1"). For unilateral experiments, the intensity of the injected-side stratum is expressed relative to the non-injected side (set to "1"). Counts of TH^+ neurons in SNpc were done in a blinded fashion using matched sections (rostra-to-caudal) across mice and treatment groups.

For the immunofluorescent staining of floating brain sections, the blocking/permeabilization, washing, and antibody-incubation steps were as described above for DAB staining, except that the quenching step was omitted and secondary antibodies were Alexa Fluor conjugates (A488 or A568) (Thermo Fisher Scientific). For confocal experiments, sections were triple stained with Alexa Fluor 488-conjugated wheat germ agglutinin (A488WGA, Thermo Fisher Scientific), TO-PRO-3 (Thermo Fisher Scientific), and antibody to TH to distinguish plasma membrane, nuclei, and DA neurons, respectively, in the SN region. A488WGA and TO-PRO-3 were included during the secondary antibody incubation step. After mounting onto slides, sections were dried briefly (3–5 min) before coverslipping with Fluoro-Gel (EMS) and sealing the coverslip with clear nail polish. Non-confocal fluorescent images were captured with either an Olympus IX70 inverted fluorescence microscope with a DP70 camera and DP Controller 2.1 software or a BX53 upright fluorescent scope with a DP72 camera and cellSens software (Olympus). ImageJ/Fiji was used to measure the fluorescence intensity of TH staining; the striatal region was outlined, the mean intensity (range of 1–255) was determined, and the mean background intensity (from the adjacent unstained region) was subtracted. Confocal images were captured using a confocal laser scanning microscope (Zeiss LSM 510 meta) with Argon 488, DPSS-561, and HeNe633 laser lines, and Zeiss ZEN software (Carl Zeiss Microscopy, White Plains, NY). Confocal images were acquired by sequential capture for each channel, with the pinhole set to 1 airy unit and matched capture conditions for injected and non-injected counterparts within sections.

mRNA-seq

mRNA-seq was performed on RNA isolated from injected and non-injected SN regions harvested 3 weeks after the stereotaxic injection of either AAV-hSYN1-miR-181 (1.65×10^{10} vg; N = 3 mice) or AAV-hSYN1-GFP (1×10^{10} vg; N = 5 mice). Total RNA samples isolated as described above were put over GeneJET RNA cleanup micro columns (cat. no. K0841, Thermo Fisher Scientific). RNA quality assessment and sequencing were performed by the Iowa Institute of Human Genetics, Genomics Division, at the University of Iowa. RNA quality and concentrations were determined with the Agilent 2100 Bioanalyzer, and DropSense or Little Lunatic (Unchained Labs, Pleasanton, CA) reads. The RNA integrity number (RIN) values for samples were >7.5. Illumina TruSeq Stranded mRNA Library Prep kits (Illumina, San Diego, CA) were used to prepare sequencing libraries from mRNA, followed by RT to cDNA, fragment purification, and ligation to indexed (barcoded) adaptors. Indexed libraries from AAV:miR-181 samples were prepared as a set and pooled for multiplex sequencing across two lanes on the Illumina HiSeq 4,000 sequencer with 75-base paired-end reads. Indexed libraries from AAV:GFP samples were prepared as a set and pooled for multiplex sequencing across 2 lanes on the Illumina NovaSeq 6,000 sequencer for 100 cycles with 50-base paired-end reads. mRNA-seq data were analyzed according to the Kallisto/Sleuth pipeline.[49,50] Reads were aligned using Kallisto version 0.43.1, to Ensemble transcriptome release 98 (119,215 transcript targets). The transcriptome was acquired on March 30,2020 from ftp://ftp.ensembl.org/pub/release-98/fasta/mus_musculus/cdna/Mus_musculus.GRCm38.cdna.all.fa.gz. Kallisto index and Kallisto quant were run using default settings, with specific

input parameters of 100 bootstraps and 16 threads. The average mapping rate across the samples was ~87% and the read depths were ~15 million reads per AAV-hSyn-GFP sample and ~40 million reads per AAV-hSyn-miR-181 sample. Differential gene expression was quantified using Sleuth version 0.30.0, aggregating abundance on Ensemble genes, with a 2-step likelihood ratio test and the Wald test. Other packages include base R version 3.6.1, biomaRt version 2.42.1, dplyr version 0.8.5, and ggplot2 version 3.2.1.

Gene Ontology analyses were performed by inputting the indicated gene sets into the ToppFun web-server tool, the ToppGene Suite,[25] and using default settings. The results were exported and up to the top 50 enriched terms in each category were tabulated in Table S2 and S3.

Statistics

Statistical analyses were performed using the available software and tools (e.g., Prism GraphPad and the R package), with guidance from the University of Iowa Department of Biostatistics.

DATA AVAILABILITY

mRNA-seq data have been deposited and made publicly available in the NCBI Gene Expression Omnibus data repository (GSE196441). All other data will be made available upon written request to the corresponding author.

SUPPLEMENTAL INFORMATION

Supplemental information can be found online at https://doi.org/10.1016/j.omtn.2022.02.007.

ACKNOWLEDGMENTS

This work was supported by funding from the Michael J. Fox Foundation for Parkinson's Research (to R.L.B.), the Roy J. Carver Trust (University of Iowa, to R.L.B.), a Iowa Neuroscience Institute Accelerator Award (University of Iowa, to R.L.B.), and the National Institutes of Health (HL148796, to R.L.B). J.M.M. was supported by the Abboud Cardiovascular Research Center NIH T32 (grant no. HL007121). We also acknowledge the University of Iowa core facilities that made significant contributions to this work, including the Viral Vector Core, Genomics Division, and Microscopy Core.

AUTHOR CONTRIBUTIONS

R.L.B. conceived and designed the project, supervised the research, and analyzed and interpreted the data. C.S.S. designed and executed the experiments, curated and analyzed the data, and participated in data interpretation. J.M.M. and N.H.W. assisted with the experiments and data collection and analyzed the data. R.L.B., C.S.S., and J.M.M. wrote the manuscript.

DECLARATION OF INTERESTS

The authors declare no competing interests.

REFERENCES

1. Singleton, A.B., Farrer, M., Johnson, J., Singleton, A., Hague, S., Kachergus, J., Hulihan, M., Peuralinna, T., Dutra, A., Nussbaum, R., et al. (2003). alpha-Synuclein locus triplication causes Parkinson's disease. Science *302*, 841.
2. Koprich, J.B., Johnston, T.H., Reyes, M.G., Sun, X., and Brotchie, J.M. (2010). Expression of human A53T alpha-synuclein in the rat substantia nigra using a novel AAV1/2 vector produces a rapidly evolving pathology with protein aggregation, dystrophic neurite architecture and nigrostriatal degeneration with potential to model the pathology of Parkinson's disease. Mol. Neurodegener *5*, 43.
3. Chesselet, M.F. (2008). *In vivo* alpha-synuclein overexpression in rodents: a useful model of Parkinson's disease? Exp. Neurol. *209*, 22–27.
4. Decressac, M., Mattsson, B., Lundblad, M., Weikop, P., and Bjorklund, A. (2012). Progressive neurodegenerative and behavioural changes induced by AAV-mediated overexpression of alpha-synuclein in midbrain dopamine neurons. Neurobiol. Dis. *45*, 939–953.
5. Thakur, P., Breger, L.S., Lundblad, M., Wan, O.W., Mattsson, B., Luk, K.C., Lee, V.M.Y., Trojanowski, J.Q., and Bjorklund, A. (2017). Modeling Parkinson's disease pathology by combination of fibril seeds and alpha-synuclein overexpression in the rat brain. Proc. Natl. Acad. Sci. United States America *114*, E8284–E8293.
6. Burgos, K., Malenica, I., Metpally, R., Courtright, A., Rakela, B., Beach, T., Shill, H., Adler, C., Sabbagh, M., Villa, S., et al. (2014). Profiles of extracellular miRNA in cerebrospinal fluid and serum from patients with Alzheimer's and Parkinson's diseases correlate with disease status and features of pathology. PLoS one *9*, e94839.
7. Briggs, C.E., Wang, Y., Kong, B., Woo, T.U., Iyer, L.K., and Sonntag, K.C. (2015). Midbrain dopamine neurons in Parkinson's disease exhibit a dysregulated miRNA and target-gene network. Brain Res. *1618*, 111–121.
8. van Rooij, E., and Kauppinen, S. (2014). Development of microRNA therapeutics is coming of age. EMBO Mol. Med. *6*, 851–864.
9. Rupaimoole, R., and Slack, F.J. (2017). MicroRNA therapeutics: towards a new era for the management of cancer and other diseases. Nat. Rev. Drug Discov. *16*, 203–222.
10. Rao, Y.S., Mott, N.N., Wang, Y., Chung, W.C., and Pak, T.R. (2013). MicroRNAs in the aging female brain: a putative mechanism for age-specific estrogen effects. Endocrinology *154*, 2795–2806.
11. Grimson, A., Farh, K.K., Johnston, W.K., Garrett-Engele, P., Lim, L.P., and Bartel, D.P. (2007). MicroRNA targeting specificity in mammals: determinants beyond seed pairing. Mol. Cel. *27*, 91–105.
12. Hegarty, S.V., Sullivan, A.M., and O'Keeffe, G.W. (2018). Inhibition of miR-181a promotes midbrain neuronal growth through a Smad1/5-dependent mechanism: implications for Parkinson's disease. Neuronal Signal *2*, NS20170181.
13. Saba, R., Storchel, P.H., Aksoy-Aksel, A., Kepura, F., Lippi, G., Plant, T.D., and Schratt, G.M. (2012). Dopamine-regulated microRNA MiR-181a controls GluA2 surface expression in hippocampal neurons. Mol. Cell. Biol. *32*, 619–632.
14. He, M., Liu, Y., Wang, X., Zhang, M.Q., Hannon, G.J., and Huang, Z.J. (2012). Cell-type-based analysis of microRNA profiles in the mouse brain. Neuron *73*, 35–48.
15. Boudreau, R.L., Jiang, P., Gilmore, B.L., Spengler, R.M., Tirabassi, R., Nelson, J.A., Ross, C.A., Xing, Y., and Davidson, B.L. (2014). Transcriptome-wide discovery of microRNA binding sites in human brain. Neuron *81*, 294–305.
16. Ghorbani, S., Talebi, F., Ghasemi, S., Jahanbazi Jahan Abad, A., Vojgani, M., and Noorbakhsh, F. (2017). miR-181 interacts with signaling adaptor molecule DENN/MADD and enhances TNF-induced cell death. PLoS one *12*, e0174368.
17. Cheng, M., Liu, L., Lao, Y., Liao, W., Liao, M., Luo, X., Wu, J., Xie, W., Zhang, Y., and Xu, N. (2016). MicroRNA-181a suppresses parkin-mediated mitophagy and sensitizes neuroblastoma cells to mitochondrial uncoupler-induced apoptosis. Oncotarget *7*, 42274–42287.
18. Indrieri, A., Carrella, S., Romano, A., Spaziano, A., Marrocco, E., Fernandez-Vizarra, E., Barbato, S., Pizzo, M., Ezhova, Y., Golia, F.M., et al. (2019). miR-181a/b downregulation exerts a protective action on mitochondrial disease models. EMBO Mol. Med. *11*, e8734.
19. Ouyang, Y.B., Lu, Y., Yue, S., Xu, L.J., Xiong, X.X., White, R.E., Sun, X., and Giffard, R.G. (2012). miR-181 regulates GRP78 and influences outcome from cerebral ischemia *in vitro* and *in vivo*. Neurobiol. Dis. *45*, 555–563.

20. Spengler, R.M., Zhang, X., Cheng, C., McLendon, J.M., Skeie, J.M., Johnson, F.L., Davidson, B.L., and Boudreau, R.L. (2016). Elucidation of transcriptome-wide microRNA binding sites in human cardiac tissues by Ago2 HITS-CLIP. Nucleic Acids Res. *44*, 7120–7131.

21. Kugler, S., Lingor, P., Scholl, U., Zolotukhin, S., and Bahr, M. (2003). Differential transgene expression in brain cells *in vivo* and *in vitro* from AAV-2 vectors with small transcriptional control units. Virology *311*, 89–95.

22. Haraguchi, T., Ozaki, Y., and Iba, H. (2009). Vectors expressing efficient RNA decoys achieve the long-term suppression of specific microRNA activity in mammalian cells. Nucleic Acids Res. *37*, e43.

23. Bell, R.D., Winkler, E.A., Sagare, A.P., Singh, I., LaRue, B., Deane, R., and Zlokovic, B.V. (2010). Pericytes control key neurovascular functions and neuronal phenotype in the adult brain and during brain aging. Neuron *68*, 409–427.

24. Albert, K., Voutilainen, M.H., Domanskyi, A., and Airavaara, M. (2017). AAV vector-mediated gene delivery to substantia nigra dopamine neurons: implications for gene therapy and disease models. Genes (Basel) *8*, 63.

25. Chen, J., Bardes, E.E., Aronow, B.J., and Jegga, A.G. (2009). ToppGene Suite for gene list enrichment analysis and candidate gene prioritization. Nucleic Acids Res. *37*, W305–W311.

26. Moore, M.J., Scheel, T.K., Luna, J.M., Park, C.Y., Fak, J.J., Nishiuchi, E., Rice, C.M., and Darnell, R.B. (2015). miRNA-target chimeras reveal miRNA 3'-end pairing as a major determinant of Argonaute target specificity. Nat. Commun. *6*, 8864.

27. Calabresi, P., Picconi, B., Tozzi, A., Ghiglieri, V., and Di Filippo, M. (2014). Direct and indirect pathways of basal ganglia: a critical reappraisal. Nat. Neurosci. *17*, 1022–1030.

28. Ford, C.P. (2014). The role of D2-autoreceptors in regulating dopamine neuron activity and transmission. Neuroscience *282*, 13–22.

29. Zhou, W., Ma, D., Sun, A.X., Tran, H.D., Ma, D.L., Singh, B.K., Zhou, J., Zhang, J., Wang, D., Zhao, Y., et al. (2019). PD-linked CHCHD2 mutations impair CHCHD10 and MICOS complex leading to mitochondria dysfunction. Hum. Mol. Genet. *28*, 1100–1116.

30. Bannwarth, S., Ait-El-Mkadem, S., Chaussenot, A., Genin, E.C., Lacas-Gervais, S., Fragaki, K., Berg-Alonso, L., Kageyama, Y., Serre, V., Moore, D.G., et al. (2014). A mitochondrial origin for frontotemporal dementia and amyotrophic lateral sclerosis through CHCHD10 involvement. Brain *137*, 2329–2345.

31. Funayama, M., Ohe, K., Amo, T., Furuya, N., Yamaguchi, J., Saiki, S., Li, Y., Ogaki, K., Ando, M., Yoshino, H., et al. (2015). CHCHD2 mutations in autosomal dominant late-onset Parkinson's disease: a genome-wide linkage and sequencing study. Lancet Neurol. *14*, 274–282.

32. Korecka, J., Schouten, M., Eggers, R., Ulusoy, A., Bossers, K., and Verhaagen, J. (2011). Comparison of AAV serotypes for gene delivery to dopaminergic neurons in the substantia nigra. Viral Gene Ther. *2*, 205–224.

33. Ulusoy, A., Decressac, M., Kirik, D., and Bjorklund, A. (2010). Viral vector-mediated overexpression of alpha-synuclein as a progressive model of Parkinson's disease. Prog. Brain Res. *184*, 89–111.

34. Theodore, S., Cao, S., McLean, P.J., and Standaert, D.G. (2008). Targeted overexpression of human alpha-synuclein triggers microglial activation and an adaptive immune response in a mouse model of Parkinson disease. J. Neuropathol. Exp. Neurol. *67*, 1149–1158.

35. Oliveras-Salva, M., Van der Perren, A., Casadei, N., Stroobants, S., Nuber, S., D'Hooge, R., Van den Haute, C., and Baekelandt, V. (2013). rAAV2/7 vector-mediated overexpression of alpha-synuclein in mouse substantia nigra induces protein aggregation and progressive dose-dependent neurodegeneration. Mol. Neurodegener *8*, 44.

36. Ren, L., Zhu, R., and Li, X. (2016). Silencing miR-181a produces neuroprotection against hippocampus neuron cell apoptosis post-status epilepticus in a rat model and in children with temporal lobe epilepsy. Genet. Mol. Res. : GMR *15*, 15017798.

37. Horst, C.H., Titze-de-Almeida, R., and Titze-de-Almeida, S.S. (2017). The involvement of Eag1 potassium channels and miR-34a in rotenone-induced death of dopaminergic SH-SY5Y cells. Mol. Med. Rep. *15*, 1479–1488.

38. Chaudhuri, A.D., Kabaria, S., Choi, D.C., Mouradian, M.M., and Junn, E. (2015). MicroRNA-7 promotes glycolysis to protect against 1-methyl-4-phenylpyridinium-induced cell death. J. Biol. Chem. *290*, 12425–12434.

39. Hu, Z.Y., Chen, B., Zhang, J.P., and Ma, Y.Y. (2017). Up-regulation of autophagy-related gene 5 (ATG5) protects dopaminergic neurons in a zebrafish model of Parkinson's disease. J. Biol. Chem. *292*, 18062–18074.

40. Carlsson, T., Schindler, F.R., Hollerhage, M., Depboylu, C., Arias-Carrion, O., Schnurrbusch, S., Rosler, T.W., Wozny, W., Schwall, G.P., Groebe, K., et al. (2011). Systemic administration of neuregulin-1beta1 protects dopaminergic neurons in a mouse model of Parkinson's disease. J. Neurochem. *117*, 1066–1074.

41. Gyllborg, D., Ahmed, M., Toledo, E.M., Theofilopoulos, S., Yang, S., Ffrench-Constant, C., and Arenas, E. (2018). The matricellular protein R-Spondin 2 promotes midbrain dopaminergic neurogenesis and differentiation. Stem Cell Rep. *11*, 651–664.

42. Hegarty, S.V., Sullivan, A.M., and O'Keeffe, G.W. (2013). BMP2 and GDF5 induce neuronal differentiation through a Smad dependant pathway in a model of human midbrain dopaminergic neurons. Mol. Cell Neurosci *56*, 263–271.

43. Han, D., Dong, X., Zheng, D., and Nao, J. (2019). MiR-124 and the underlying therapeutic promise of neurodegenerative disorders. Front Pharmacol. *10*, 1555.

44. Zhao, M.W., Yang, P., and Zhao, L.L. (2019). Chlorpyrifos activates cell pyroptosis and increases susceptibility on oxidative stress-induced toxicity by miR-181/SIRT1/PGC-1alpha/Nrf2 signaling pathway in human neuroblastoma SH-SY5Y cells: implication for association between chlorpyrifos and Parkinson's disease. Environ. Toxicol. *34*, 699–707.

45. Gu, C., Shen, J., Zhang, F., and Chen, J. (2017). MicroRNA-181a knockdown protects HepaRG cells from Dichlorvos-induced oxidative stress and apoptosis. Int. J. Clin. Exp. Pathol. *10*, 10883–10891.

46. Wang, X., Zhou, S., Ding, X., Zhu, G., and Guo, J. (2010). Effect of triazophos, fipronil and their mixture on miRNA expression in adult zebrafish. J. Environ. Sci. Health B *45*, 648–657.

47. Paxinos, G., and Franklin, K.B.J. (2001). The Mouse Brain in Stereotaxic Coordinates (San Diego: Academic Press).

48. Lee, B.R., and Kamitani, T. (2011). Improved immunodetection of endogenous alpha-synuclein. PLoS one *6*, e23939.

49. Bray, N.L., Pimentel, H., Melsted, P., and Pachter, L. (2016). Near-optimal probabilistic RNA-seq quantification. Nat. Biotechnol. *34*, 525–527.

50. Pimentel, H., Bray, N.L., Puente, S., Melsted, P., and Pachter, L. (2017). Differential analysis of RNA-seq incorporating quantification uncertainty. Nat. Methods *14*, 687–690.